



HAL
open science

Simple rules govern the diversity of bacterial nicotianamine-like metallophores

Clémentine Laffont, Catherine Brutesco, Christine Hajjar, Gregorio Cullia,
Roberto Fanelli, Laurent Ouerdane, Florine Cavelier, Pascal Arnoux

► **To cite this version:**

Clémentine Laffont, Catherine Brutesco, Christine Hajjar, Gregorio Cullia, Roberto Fanelli, et al.. Simple rules govern the diversity of bacterial nicotianamine-like metallophores. *Biochemical Journal*, 2019, 476 (15), pp.2221-2233. 10.1042/bcj20190384 . cea-02275929

HAL Id: cea-02275929

<https://cea.hal.science/cea-02275929>

Submitted on 3 Sep 2019

HAL is a multi-disciplinary open access archive for the deposit and dissemination of scientific research documents, whether they are published or not. The documents may come from teaching and research institutions in France or abroad, or from public or private research centers.

L'archive ouverte pluridisciplinaire **HAL**, est destinée au dépôt et à la diffusion de documents scientifiques de niveau recherche, publiés ou non, émanant des établissements d'enseignement et de recherche français ou étrangers, des laboratoires publics ou privés.

1 **Simple rules govern the diversity of bacterial nicotianamine-like metallophores**

2 Clémentine Laffont¹, Catherine Brutesco¹, Christine Hajjar¹, Gregorio Cullia², Roberto Fanelli²,
3 Laurent Ouerdane³, Florine Cavelier², Pascal Arnoux^{1,*}

4 ¹Aix Marseille Univ, CEA, CNRS, BIAM, Saint Paul-Lez-Durance, France F-13108.

5 ²Institut des Biomolécules Max Mousseron, IBMM, UMR-5247, CNRS, Université Montpellier,
6 ENSCM, Place Eugène Bataillon, 34095 Montpellier cedex 5, France.

7 ³CNRS-UPPA, Laboratoire de Chimie Analytique Bio-inorganique et Environnement, UMR 5254,
8 Hélioparc, 2, Av. Angot 64053 Pau, France.

9 ***Correspondance:** Pascal Arnoux, Aix Marseille Univ, CEA, CNRS, BIAM, Saint Paul-Lez-
10 Durance, France F-13108; pascal.arnoux@cea.fr; Tel. 04-42-25-35-70

11 **Keywords:** opine/opaline dehydrogenase, CntM, nicotianamine-like metallophore, bacillopaline

12 13 **ABSTRACT**

14 In metal-scarce environments, some pathogenic bacteria produce opine-type metallophores
15 mainly to face the host's nutritional immunity. This is the case of staphylopine, pseudopaline and
16 yersinopine, identified in *Staphylococcus aureus*, *Pseudomonas aeruginosa* and *Yersinia pestis*
17 respectively. Depending on the species, these metallophores are synthesized by two (CntLM) or three
18 enzymes (CntKLM), CntM catalyzing the last step of biosynthesis using diverse substrates (pyruvate
19 or α -ketoglutarate), pathway intermediates (xNA or yNA) and cofactors (NADH or NADPH). Here,
20 we explored substrate specificity of CntM by combining bioinformatics and structural analysis with
21 chemical synthesis and enzymatic studies. We found that NAD(P)H selectivity was mainly due to the
22 amino acid at position 33 (*S. aureus* numbering) which ensures a preferential binding to NADPH
23 when it is an arginine. Moreover, whereas CntM from *P. aeruginosa* preferentially uses yNA over
24 xNA, the staphylococcal enzyme is not stereospecific. Most importantly, selectivity towards α -
25 ketoacids is largely governed by a single residue at position 150 of CntM (*S. aureus* numbering): an
26 aspartate at this position ensures selectivity towards pyruvate whereas an alanine leads to the
27 consumption of both pyruvate and α -ketoglutarate. Modifying this residue in *P. aeruginosa* led to a
28 complete reversal of selectivity. Thus, opine-type metallophore diversity is governed by the
29 absence/presence of a *cntK* gene encoding a histidine racemase, and the amino acid residue at position
30 150 of CntM. These two simple rules predict the production of a fourth metallophore by *Paenibacillus*
31 *mucilaginosus*, which was confirmed *in vitro* and called bacillopaline.

32 33 34 **INTRODUCTION**

35 In metal-scarce environments, bacteria have to use efficient mechanisms for the uptake of
36 metals required for their growth. This is particularly the case for pathogenic bacteria that have to
37 confront the host's immune system. Indeed, the so-called "nutritional immunity" induces an additional
38 metal limitation by sequestering iron, zinc or manganese to prevent bacterial growth [1–4]. To face
39 this metal restriction, bacteria have developed metallophores to recover metals. In this context,
40 nicotianamine-like metallophores have been identified in some bacteria as playing an important role in
41 metal acquisition strategies. Staphylopine, pseudopaline and yersinopine are the three examples

42 currently known and recently identified in *S. aureus* [5], *P. aeruginosa* [6,7] and *Y. pestis* [8]
43 respectively. Depending on the species, the biosynthesis of these nicotianamine-like metallophores
44 occurs in two or three steps. When it is present, such as in *S. aureus*, CntK, a histidine racemase,
45 transforms L-histidine (L-His) into D-histidine (D-His). CntL, a nicotianamine synthase-like, adds an
46 aminobutyrate moiety coming from S-adenosyl methionine (SAM) on the amino group of its second
47 substrate (L-His in *P. aeruginosa* and *Y. pestis* or D-His in *S. aureus*) to form a pathway intermediate
48 (noted yNA when using L-His, xNA when using D-His). Finally, CntM, an enzyme belonging to the
49 opine dehydrogenase family, condenses the pathway intermediate with an α -ketoacid (pyruvate in the
50 case of *S. aureus* and *Y. pestis* or α -ketoglutarate (α KG) in the case of *P. aeruginosa*) using NAD(P)H
51 to form an opine-type metallophore (Figure 1).

52 Opine dehydrogenase catalyzes the NAD(P)H-dependent reductive condensation of the amino
53 group of an amino acid with an α -ketoacid to produce an N-(carboxyalkyl) amino acid, also known as
54 an opine, which exhibits either (L,L) or (D,L) stereochemistry [9]. The variety of amino acids and α -
55 ketoacids that can be used as substrates by opine dehydrogenases results in diverse products. For
56 example, the octopine dehydrogenase catalyzes the production of octopine, lysopine or histopine *via*
57 reductive condensation of pyruvate and L-arginine, L-lysine and L-histidine respectively [10–13].
58 Leucinopine, asparaginopine and glutaminopine are other examples of opines produced *via* reductive
59 condensation of α -ketoglutarate with L-leucine, L-asparagine and L-glutamine respectively [14,15]. In
60 addition to the diversity of substrates, opine dehydrogenases are also distinguished by their biological
61 roles. Indeed, in some marine invertebrates, opine dehydrogenases participate in the anaerobic
62 metabolism by insuring the last step of anaerobic glycolysis pathway therefore participating in the
63 propelling of these animals [16,17]. In plants, diverse opines are found inside crown gall tumors (for
64 example nopaline, agropine, octopine, mannopine or D-L and L-L-succinamopine) that are induced by
65 plant pathogenic bacteria as *Agrobacterium tumefaciens* [18,19] In this case, the opines serve as
66 nutrients conferring selective growth advantages to the opine-producing and opine-utilizing
67 microorganisms [20–22].

68 Opine dehydrogenases are also involved in the biosynthesis of nicotianamine-like
69 metallophores in bacteria and their substrate specificity results in the production of diverse
70 metallophores. The activity of these opine dehydrogenases from *S. aureus*, *P. aeruginosa* and *Y. pestis*
71 (respectively called SaCntM, PaCntM and YpCntM) has been described: SaCntM uses NADPH and
72 pyruvate with xNA to produce staphylopin [5], YpCntM uses pyruvate and NADPH with yNA to
73 produce yersinopine [8], and PaCntM uses NAD(P)H and α -ketoglutarate with yNA to produce
74 pseudopaline [6,7]. Therefore, substrate specificity (and eventually stereospecificity in the case of
75 xNA *vs* yNA) of CntM leads to the production of diverse opine-type metallophores. These
76 metallophores are involved in metal acquisition, with metal specificity depending on the growth
77 medium. Staphylopin could transport copper, nickel, cobalt, zinc and iron [5,23,24], and participates
78 in zinc uptake in zinc-scarce environments [23,25]. Pseudopaline is involved in nickel uptake in
79 minimal media, whereas it is responsible for zinc uptake in zinc-scarce environment [6,26]. For both
80 *S. aureus* and *P. aeruginosa*, literature reports a link between the production of opine-type
81 metallophores and bacterial infection. For example, in *S. aureus*, the staphylopin receptor CntA plays
82 an important role in the optimal functioning of the urease activity and is ultimately linked to its
83 virulence as the deletion of the gene encoding this substrate binding protein leads to a decrease of
84 murine bacteremia and urinary tract infections [24]. In *P. aeruginosa*, transcriptomic analyses showed
85 that the biosynthetic genes for pseudopaline are overexpressed in burn wound infections in humans
86 [27]. This overexpression would make it possible to bypass the metal limitations put in place during
87 nutritional immunity. Moreover, the pseudopaline exporter CntI plays an important role in the survival
88 and growth of *P. aeruginosa* in cystic fibrosis airway: deletion of the gene encoding this exporter
89 resulted in an attenuation of this respiratory infection [28]. Similarly, the exporter of staphylopin was

90 found to be important for fitness in abscesses, even before staphylopin discovery [29]. Concerning *Y.*
91 *pestis*, no data indicates a link between yersinopine production and virulence at this time and the
92 discovery of this metallophore is so far restricted to *in vitro* studies [8].

93 In an effort to understand bacterial opine-type metallophore diversity, we studied substrate
94 specificity of CntM in *S. aureus* and *P. aeruginosa* by combining bioinformatic and structural analyses
95 with chemical synthesis and enzymatic studies. We found that a single amino acid residue was
96 responsible for the preferential binding of NADPH, and a single residue was involved in the
97 specificity towards pyruvate or α -ketoglutarate. This finding led us to establish simple rules involved
98 in opine-type metallophore diversity and prompted us to dig into available genomes for a bacteria
99 possessing a *cntK* homologue together with a *cntM* gene predicted to use α -ketoglutarate. This
100 exploration ultimately led to the discovery of a new opine-type metallophore called bacillopaline in
101 *Paenibacillus mucilaginosus*.

103 MATERIALS AND METHODS

104 Bioinformatic analyses

105 SaCntM (*sav2468*) protein sequence was analyzed by searching for homologues using Psi-
106 BLAST search [30] through the NCBI databases (National Center for Biotechnology Information,
107 Bethesda, Maryland, USA) and the Pfam database (European Bioinformatics Institute, Hinxton,
108 England, UK). Sequence alignment was done using the Muscle program [31] with defaults criteria
109 from Jalview (version 2.10.3) [32]. Residues were colored following the Clustal coloring scheme with
110 intensity modified by a conservation color increment of 30%. Gene synteny were inspected using the
111 MaGe MicroScope web interface [33] added to sequence alignment analysis.

112 Cloning, expression and purification of proteins

113 The gene encoding the SaCntM protein were cloned in pET-SUMO and pET-101 [5,34] and
114 the one encoding the PaCntM protein were cloned in pET-TEV [6]. Similarly, the genes encoding the
115 PmCntL and PmCntM proteins were cloned in pET-TEV from genomic DNA. The primers used for
116 these constructions are listed in Table S1. After co-transformation with plasmid pRARE (encoding for
117 rare codon in *E. coli*), *E. coli* BL21 strains were aerobically cultivated with horizontal shaking in LB
118 media supplemented with appropriate antibiotics (kanamycin at 50 $\mu\text{g}\cdot\text{mL}^{-1}$ for pET-SUMO and pET-
119 TEV, ampicillin at 50 $\mu\text{g}\cdot\text{mL}^{-1}$ for pET-101 and chloramphenicol at 25 $\mu\text{g}\cdot\text{mL}^{-1}$ for pRARE). These
120 strains were grown in diverse conditions (37°C or 16°C, with or without induction of protein
121 expression by addition of 0.1 mM IPTG when the OD of the culture was about 0.6; Table S2). After
122 overnight growth, cells were recovered by centrifugation at 5,000 g for 20 min at 4°C. Cells were
123 resuspended in buffer A and disrupted using a Constant cell disruption system operating at 1.9 Kbar.
124 Cell debris were removed by centrifugation at 8,000 g for 20 min. The supernatant was centrifuged at
125 100,000 g for 45 min at 4°C to remove cell wall debris and membrane proteins. The resulting soluble
126 fraction was purified by batch using a nickel-charged affinity resin (Ni-NTA Agarose resin,
127 ThermoFisher Scientific). The proteins were eluted stepwise with imidazole (15 mM wash, 250 mM or
128 500 mM elution). Collected fractions were transferred into imidazole-free buffer B (see Table S2 for
129 details on the buffers used and Figure S8 for the monitoring of protein purifications).

130 Site directed mutagenesis

131 Site directed mutagenesis were performed according to standard protocol from the
132 QuickChange II Site-Directed Mutagenesis kit (Agilent Technologies). The only difference was that *E.*
133 *coli* DH10 β Competent Cells were used instead of XL1-Blue Supercompetent Cells for

134 transformations. Selection of colonies was done after spreading on LB plate supplemented with
135 appropriate antibiotics. Plasmid pET-SUMO containing the gene encoding the SaCntM protein and
136 plasmid pET-TEV containing the gene encoding the PaCntM protein were used as mutagenesis
137 templates for the D150A and A153D substitutions respectively. For the R33H substitution from
138 SaCntM, mutagenesis was performed from plasmid pET-101 containing the gene encoding the
139 SaCntM protein as template. Primer pairs were designed for single substitutions and were then
140 synthesized by Eurofins Genomics (Table S1).

141 **Chemical synthesis of xNA and yNA**

142 The chemical synthesis of xNA has recently been described [34]. The same strategy was used
143 for the chemical synthesis of yNA, although L-His-OMe was used instead of D-His-OMe as starting
144 material. Purified intermediates and their characterization are described in the supplementary
145 materials.

146 **CntM activity assay**

147 Enzymatic reactions of CntM were performed at 28°C in microplates and with purified
148 proteins. They were carried out in a reaction volume of 100 µL in buffer C (50 mM BisTrisPropane,
149 100 mM NaCl, pH = 7 for SaCntM and PmCntM or pH = 8 for PaCntM) containing 2 or 5 µg of
150 enzyme, 0.2 mM of NADH or NADPH (Sigma-Aldrich), 0.2 mM of xNA or yNA (chemically
151 synthesized), and 1 mM of pyruvate or α-ketoglutarate (Sigma-Aldrich), unless otherwise stated. The
152 absorbance at 340 nm was measured using a microplate reader (Infinite 200 Pro; Tecan) to follow the
153 oxidation of NADPH illustrating the progress of the reaction. Activities were calculated from the
154 initial rate and the amount of enzyme used. Kinetic parameters were estimated according to the
155 Michaelis-Menten kinetic without (1) or with the substrate inhibition model (2) using SigmaPlot.
156 These values were used to plot a fit on the experimental data. (V_m : Maximum velocity; K_m : Michaelis
157 constant; $[S]$: substrate concentration; K_i : Inhibition constant).

158 (1):
$$v = \frac{v_m [S]}{K_m + [S]}$$

159 (2):
$$v = \frac{v_m [S]}{K_m + [S](1 + \frac{[S]}{K_i})}$$

160

161 **Fluorescence resonance energy transfer (FRET) studies**

162 Fluorescence studies were performed using a Cary Eclipse spectrophotometer (Agilent). The
163 FRET experiment was done using a protein concentration of 5 µM and an excitation wavelength at
164 280 nm (tryptophan excitation). The emission at 340nm was transferred to the NAD(P)H and the
165 signal was recorded between 400 and 500 nm. Five spectra were averaged in order to increase signal
166 to noise ratio.

167 **Activity assay followed by TLC**

168 The assay consisted in incubating the purified enzymes at a final concentration of 2.5 µM and
169 using carboxyl-¹⁴C-labeled SAM (2.5 µM), NADPH or NADH (30 µM), L- or D-histidine (10 µM)
170 and α-keto acid (pyruvate or α-ketoglutarate; 1mM). The total volume was 100 µL in buffer D (50 mM
171 of HEPES, 1 mM of DTT, 1mM of EDTA, pH = 9). The mixtures were incubated for 30 min at 28 °C.
172 The reactions were stopped by adding ethanol to a final concentration of 50 % (v/v) and the products
173 were then separated by thin layer chromatography. An aliquot of 10 µL of the reaction mixtures were
174 spotted on HPTLC (High Performance TLC) Silica Gel 60 Glass Plates (Merck KGaA), and the plates
175 were developed with a phenol:n-butanol:formate:water (12:3:2:3 v/v) solvent system. These separation

176 parameters were used in the initial biochemical characterization of plant nicotianamine synthase [35]
177 and of staphylopine and pseudopaline [5,6]. HPTLC plates were dried and exposed to a [¹⁴C]-sensitive
178 imaging plate for one day. Imaging plates were then scanned on a Typhoon FLA 7000
179 phosphorimager (GE Healthcare).

180

181 **Cell culture conditions of *Paenibacillus mucilaginosus***

182 *Paenibacillus mucilaginosus*, sub sp. 1480D (from DSMZ collection) was grown by
183 inoculating stock bacteria into 20 mL sterile medium (TSB 1/10) at 30°C for 48h. Genomic DNA was
184 extracted using the protocols and pretreatments for Gram-positive bacteria from DNeasy Blood and
185 Tissue kit (Qiagen).

186

187 **RESULTS AND DISCUSSION**

188 **Specificity towards NADH or NADPH**

189 The structure of CntM has been solved in a binary/tertiary complex with NADPH or NADPH
190 and xNA, revealing the residues that are involved in the complex formation and building the active
191 site [8,34] (pdb code 6C4T and 6H3D, respectively). Focusing on the NADPH binding site of SaCntM
192 we observed that the phosphate group of NADPH is sandwiched by the side chains of two positively
193 charged residues (R33 and K39) that are rather conserved in the CntM family (Figure 2A). However, a
194 sequence alignment of nine CntM homologues shows that R33 residue in SaCntM is conserved in
195 YpCntM, but replaced by a histidine in PaCntM (Figure 2B). As it is known that SaCntM and
196 YpCntM specifically use NADPH [5,8] while PaCntM can use NADH or NADPH [6–8], we
197 hypothesized that the nature of the amino acid residue at this position could determine the
198 NADH/NADPH selectivity by CntM.

199 We therefore sought to determine the role of this residue in NAD(P)H selectivity by replacing
200 this arginine by a histidine in a SaCntM:R33H variant. Because the histidine could either be neutral or
201 positively charged at pH above or below its pK_a, the binding of NAD(P)H was followed at two pHs
202 (6.0 and 8.5). We found that the WT enzyme, whatever the pH, still preferentially binds NADPH over
203 NADH (Figure 3). On the contrary, the R33H mutant behaves as the WT at pH 6.0, whereas it loses its
204 preferential binding property at a higher pH. This shows that a histidine at this position could serve as
205 a selective residue, stabilizing NADPH at acidic pH when the imidazole ring of histidine is positively
206 charged, and favoring NADH binding when histidine is neutral at basic pH, overall explaining the
207 difference of selectivity in the literature [6–8]. In other words, at acidic pH the histidine side chain of
208 the R33H mutant is charged and behaves like the WT, whereas at basic pH this histidine is neutral, it
209 could not form a salt bridge with the phosphate of NADPH and therefore could not discriminate
210 between NADPH and NADH. Interestingly, we noted that *Fictibacillus arsenicus* possesses a histidine
211 residue at the conserved position equivalent to K39 in *S. aureus*, suggesting the same possibility of
212 preferential NADH binding at basic pH.

213 **Specificity towards xNA or yNA**

214 *In vivo*, CntM uses the product of CntL *i.e.* xNA or yNA depending on the species. However,
215 using enzymatically produced xNA or yNA, McFarlane *et al.* (2018) suggested that SaCntM could use
216 both diastereoisomers. Activities from *S. aureus* (SaCntM) and from *P. aeruginosa* (PaCntM) were
217 therefore compared for their ability to use chemically synthesized xNA and yNA as substrate (Figure
218 4). The chemical synthesis of xNA was recently reported [34] and we were able to synthesize yNA by
219 following the same approaches (see the experimental procedures and the supplementary materials).
220 Reactions were then performed *in vitro* using purified proteins and a concentration range of xNA and
221 yNA with a saturating concentration of other substrates: 0.2 mM of NADPH and 1 mM of pyruvate

222 (when evaluating SaCntM) or α -ketoglutarate (when evaluating PaCntM). Overall, we found that the
223 activity of CntM from *S. aureus* and *P. aeruginosa* towards yNA and xNA were different. In the case
224 of SaCntM, although xNA is used *in vivo* to produce staphylopin, its activity is higher when using
225 yNA *in vitro*. Indeed, the k_{cat} for the reaction with yNA is ~ 2 -fold higher than the one with xNA (3.18
226 s^{-1} and 1.67 s^{-1} respectively). However, the K_{m} for the reaction with yNA is ~ 2 -fold higher than the
227 one with xNA (47 μM and 23 μM respectively), leading to a catalytic efficiency ($k_{\text{cat}}/K_{\text{m}}$) of the same
228 order of magnitude for the two substrates (Table 1). In the case of PaCntM, the enzyme uses yNA to
229 produce pseudopaline *in vivo*. In agreement with this, we found that the reaction with yNA is more
230 efficient than the one with xNA, the reaction with yNA exhibiting a catalytic efficiency ~ 10 -fold
231 higher than with xNA (29 618 $\text{M}^{-1}\text{s}^{-1}$ and 2 918 $\text{M}^{-1}\text{s}^{-1}$ respectively).

232 In the past decades, several opine dehydrogenases have been studied and their biosynthetic
233 reactions generally exhibit a substrate stereospecificity towards the amino group with most enzymes
234 using the L-stereoisomer as substrate [9]. For example, substrate stereospecificity has been outlined
235 for the octopine dehydrogenase from *Pecten maximus* [12] and the structure of this enzyme shows a
236 negatively charged cavity acting as a “charge ruler”, which favors L-arginine binding. Here, we found
237 that even if SaCntM uses xNA *in vivo*, it is also capable of using yNA *in vitro*. This trend confirms the
238 one outlined by McFarlane *et al.* [8] using enzymes from different species. Under their experimental
239 conditions, PaCntM exhibited a k_{cat} of 0.016 s^{-1} in the presence of xNA, which was biosynthesized
240 with SaCntL. Accordingly, we found that PaCntM preferentially used yNA whether *in vitro* or *in vivo*.
241 All these data therefore suggest that there is a substrate stereospecificity in the case of PaCntM, which
242 is not found in SaCntM. We further noted that, using yNA but not xNA, a drop in enzyme activity is
243 visible at high substrate concentrations, which suggests a mechanism of substrate inhibition (Figure 4).
244 Indeed, the fits made with a substrate inhibition model added to the Michaelis-Menten kinetic better
245 cover the experimental data (Figure 4; plain lines). However, this substrate inhibition is not visible
246 when using xNA as substrate.

247 **Specificity towards pyruvate or α -ketoglutarate**

248 In order to find amino acid residues involved in the pyruvate/ α -ketoglutarate selectivity by
249 CntM, we searched for residues located in the vicinity of the active site (*i.e.* the nicotinamide moiety)
250 and conserved in species known to use pyruvate (*S. aureus* and *Y. pestis*) but differing in species
251 known to use α -ketoglutarate (*P. aeruginosa*). This pointed to the aspartic acid residue at position 150
252 in SaCntM, which is also present in YpCntM but replaced by an alanine in PaCntM (corresponding to
253 residue 153 in this enzyme). Because this residue is either an aspartic acid or an alanine, we
254 hypothesized that the nature of the amino acid residue at this position would determine the pyruvate/ α -
255 ketoglutarate selectivity by CntM. This postulate was also proposed by McFarlane *et al.* [8]. In order
256 to test the role of this amino acid in pyruvate/ α -ketoglutarate selectivity, we replaced the aspartic acid
257 by an alanine in SaCntM (D150A variant) and did the opposite mutation in PaCntM (A153D). The
258 activities of these proteins were then compared for their ability to use of pyruvate and α -ketoglutarate
259 as substrates (Figure 5 and Figure S8 for the monitoring of protein purifications). The reactions were
260 performed using a concentration range of pyruvate and α -ketoglutarate with a fixed concentration of
261 others substrates: 0.2 mM of NAD(P)H and 0.2 mM of xNA (when using SaCntM) or yNA (PaCntM).
262 As a control, we verified that the mutation did not affect the binding of the NADPH on SaCntM
263 (Figure S9).

264 With regard to SaCntM, we confirmed that the WT was only able to use pyruvate, with a k_{cat} of 1.0 s^{-1}
265 and a K_{m} of 51 μM , resulting in a catalytic efficiency of 19 592 $\text{M}^{-1}\text{s}^{-1}$ (Figure 5 and Table 2). On the
266 contrary, the D150A variant of SaCntM could use both pyruvate and α -ketoglutarate as substrates.
267 Indeed, although the maximum activity is not reached within the concentration range tested, the
268 kinetic parameters calculated for both pyruvate and α -ketoglutarate are in the same order of
269 magnitude. This single substitution therefore led to a decreased activity when using pyruvate but most

270 of all, significantly led to an increased activity when using α -ketoglutarate. Even if we take a lower
271 limit for the k_{cat} of 1.65 s^{-1} for α -ketoglutarate, this would correspond to a more than 40-fold increased
272 as compared to the WT SaCntM. We then investigated whether the opposite mutation in PaCntM
273 would trigger the opposite effect on substrate selectivity. Here again, we confirmed that the WT
274 enzyme could only use α -ketoglutarate with a k_{cat} of 0.27 s^{-1} and a K_{m} of $133 \mu\text{M}$. Strikingly, we found
275 that the A153D substitution in PaCntM led to a complete reversal of selectivity, with the variant only
276 being able to use pyruvate and unable to use α -ketoglutarate anymore. This mutation is indeed
277 accompanied by a more than 20-fold increase in k_{cat} for pyruvate and ~ 30 -fold decrease for α -
278 ketoglutarate, *i.e.* a complete switch in substrate specificity. Consequently, substrate specificity of
279 CntM towards pyruvate or α -ketoglutarate is mainly governed by this single amino acid (position 150
280 in SaCntM or 153 in PaCntM): an aspartate ensures the selection of pyruvate whereas an alanine leads
281 to α -ketoglutarate specificity. To our knowledge, this is the first example showing that substrate
282 specificity might be tuned in opine/opaline dehydrogenases family. There are however some examples
283 of redesigned substrate specificity in dehydrogenases such as the production of a highly active malate
284 dehydrogenase starting from lactate dehydrogenase [36]. In this case, the Gln102Arg mutation of
285 *Bacillus stearothermophilus* lactate dehydrogenase led to a shift in $k_{\text{cat}}/K_{\text{m}}$ with malate so that it equal
286 that of native lactate dehydrogenase for its natural substrate. Examples of site directed mutagenesis
287 studies in the opine/opaline family were centered on the catalytic residues and all led to decreased
288 activities towards substrates and none explored the putative α -ketoacid specificity [12,37]. Finally,
289 there is also an example of opine binding proteins in which a single residue is key to the recognition of
290 pyruvate vs α KG opines (*ie* octopines vs nopaline) [38].
291

292 **Identification of a novel nicotianamine-like metallophore**

293 Having established the molecular determinant for the α -ketoacid selectivity of CntM, we
294 propose two simple rules governing the production of nicotianamine-like metallophores: 1) the
295 presence or absence of a *cntK* homologue, which may or may not lead to the production of D-His from
296 L-His respectively (then used by CntL to produce xNA or yNA respectively), and 2) the presence of
297 an aspartate or an alanine at position 150 (*S. aureus* numbering), which results in pyruvate or α -
298 ketoglutarate incorporation, respectively. Applying these rules, we searched for a species capable of
299 producing the missing metallophore variant, which would use xNA and incorporate α -ketoglutarate,
300 *i.e.* a species possessing a *cntK* homologue and an alanine at position responsible for α -ketoglutarate
301 selectivity. Digging into available genomes *in silico*, we identified *Paenibacillus mucilaginosus* as a
302 good candidate. Indeed, this species carries an A153 in CntM (as *P. aeruginosa*) and possess a *cntK* in
303 its *cnt* operon (as *S. aureus*) (Figure 2B-C).

304 To check the validity of this hypothesis, genes encoding the CntL and CntM from *P.*
305 *mucilaginosus* (PmCntL and PmCntM respectively) were amplified from genomic DNA, cloned in
306 expression vectors, purified and used to determine the substrates they consumed *in vitro* (Figure 6).
307 Enzymes activities were first assayed using TLC separation, using carboxyl- $[^{14}\text{C}]$ -labeled SAM
308 substrate. In this assay, $[^{14}\text{C}]$ -labeled SAM shows a characteristic profile with one strong band and two
309 others bands of much lower intensity (Figure 6 A). The incubation of $[^{14}\text{C}]$ -labeled SAM with PmCntL
310 led to another prominent band in the presence of D-His, which was not found using L-His. This novel
311 band migrated below the SAM band and therefore corresponds to the xNA intermediate. This indicates
312 that PmCntL uses D-His and not L-His, and further validates the link between the presence of a *cntK*
313 gene and the use of D-His by CntL. We then tested the substrate specificity of PmCntM by co-
314 incubating both PmCntL and PmCntM together with diverse substrates: pyruvate or α -ketoglutarate
315 with NADH or NADPH. When using NADPH and D-His with either pyruvate or α -ketoglutarate, we
316 neither detected the SAM nor xNA pattern, but found a novel band migrating just above the SAM in
317 the presence of pyruvate (which corresponds to staphylopine) and just below the SAM in the presence
318 of α -ketoglutarate. Surprisingly, we thus found that PmCntM could use both pyruvate and α -
319 ketoglutarate in this TLC assay. However, TLC experiments were run using a defined incubation time

320 (30 min), which might hinder differences in enzyme efficiency. We therefore determined the
321 enzymatic parameters of PmCntM using purified protein and a concentration range of pyruvate and α -
322 ketoglutarate, with a fixed concentration of others substrates: 0.2 mM of NADPH and 0.2 mM of xNA
323 (Figure 6 B). As a result, we found that the catalytic efficiency is 10-fold better for α -ketoglutarate
324 than for pyruvate ($10\,367\text{ M}^{-1}\text{s}^{-1}$ and $1\,016\text{ M}^{-1}\text{s}^{-1}$ respectively; Table 3). These data therefore suggest
325 that our hypothesis is valid: CntL and CntM from *P. mucilaginosus* produce an additional variant of
326 opine-type metallophore with D-His, NADPH and α -ketoglutarate. This metallophore has been called
327 bacillopaline as it belongs to the opaline family (Figure 6 C). Moreover, we found that, in addition to
328 using both pyruvate and α -ketoglutarate, CntM from *P. mucilaginosus* is also able to use both xNA
329 and yNA (Figure S10, Table S3).

330 Contrary to human pathogens like *S. aureus*, *P. aeruginosa* or *Y. pestis* in which opine-type
331 metallophores were discovered [5–8], *P. mucilaginosus* is a soil bacteria. The production of opine-type
332 metallophores was shown to be regulated by zinc through the zur (zinc uptake repressor) repressor
333 [6,25], which is likely the case in *P. mucilaginosus*, with a putative zur box upstream the *cnt* operon.
334 A possible hypothesis would be that bacillopaline production could be induced in calcareous soils,
335 where zinc bioavailability has been shown to be low [39]. In the past decade, *P. mucilaginosus* have
336 been studied for its capacity in wastewater treatment, but also as biofertilizer and plant growth
337 promoting rhizobacteria [40–42]. Indeed, in addition to producing biofloculants or plant hormones,
338 this species is able to solubilize phosphates, to fix nitrogen and to produce ammonia. Moreover, it is
339 able to produce siderophores, which contributes to plant growth by indirectly preventing the growth of
340 plant pathogens [41,43]. Similarly, we could hypothesize that bacillopaline could contribute in the
341 same way to maintain plant micronutrients homeostasis.

342 In conclusion, studying the substrate specificity of the enzyme catalyzing the last step of
343 nicotianamine-like metallophore biosynthesis allowed us to determine simple rules governing their
344 production. First, the presence or absence of a *cntK* gene leads to the use of respectively D-His or L-
345 His by CntL resulting in the incorporation of respectively xNA or yNA by CntM. Secondly, the
346 presence of an aspartate or an alanine at position 150 on CntM (*S. aureus* numbering) results in
347 pyruvate or α -ketoglutarate incorporation, respectively. Thanks to these simple rules, it is now possible
348 to predict the nature of the nicotianamine-like metallophore produced by all bacteria possessing a *cnt*
349 operon in their genome.

350

351 Acknowledgments

352 We thank the Agence Nationale de la Recherche (grant ANR-14-CE09-0007-02) for initial support
353 and the association Vaincre la Mucoviscidose (VLM, grant RFI20160501495) for financial support.

354

355 Conflict of Interest

356 The authors declare that they have no conflicts of interest with the contents of this article.

357

358 Author contributions

359 C.L. and P.A. designed the experiments. C.L., C.B., C.H. and L.O. carried out the experiments. C.L.,
360 C.B. and P.A. analyzed the data. G.C, R.F synthesized xNA and yNA under the supervision of F.C.
361 C.L. and P.A. wrote the manuscript with contributions from F.C.

362

363 References

364 1 Capdevila, D. A., Wang, J. and Giedroc, D. P. (2016) Bacterial Strategies to Maintain Zinc
365 Metallostatics at the Host-Pathogen Interface. *J. Biol. Chem.* **291**, 20858–20868.

- 366 2 Hood, M. I. and Skaar, E. P. (2012) Nutritional immunity: transition metals at the pathogen–host
367 interface. *Nat. Rev. Microbiol.* **10**, 525–537.
- 368 3 Weinberg, E. D. (1975) Nutritional immunity. Host’s attempt to withhold iron from microbial
369 invaders. *JAMA* **231**, 39–41.
- 370 4 Zygiel, E. M. and Nolan, E. M. (2018) Transition Metal Sequestration by the Host-Defense Protein
371 Calprotectin. *Annu. Rev. Biochem.* **87**, 621–643.
- 372 5 Ghssein, G., Brutesco, C., Ouerdane, L., Fojcik, C., Izaute, A., Wang, S., Hajjar, C., Lobinski, R.,
373 Lemaire, D., Richaud, P., et al. (2016) Biosynthesis of a broad-spectrum nicotianamine-like
374 metallophore in *Staphylococcus aureus*. *Science* **352**, 1105–1109.
- 375 6 Lhospice, S., Gomez, N. O., Ouerdane, L., Brutesco, C., Ghssein, G., Hajjar, C., Liratni, A., Wang, S.,
376 Richaud, P., Bleves, S., et al. (2017) *Pseudomonas aeruginosa* zinc uptake in chelating
377 environment is primarily mediated by the metallophore pseudopaline. *Sci. Rep.* **7**.
- 378 7 McFarlane, J. S. and Lamb, A. L. (2017) Biosynthesis of an Opine Metallophore by *Pseudomonas*
379 *aeruginosa*. *Biochemistry* **56**, 5967–5971.
- 380 8 McFarlane, J. S., Davis, C. L. and Lamb, A. L. (2018) Staphylopine, pseudopaline, and yersinopine
381 dehydrogenases: A structural and kinetic analysis of a new functional class of opine
382 dehydrogenase. *J. Biol. Chem.* **293**, 8009–8019.
- 383 9 Thompson, J. and Donkersloot, J. A. (1992) N-(Carboxyalkyl)Amino Acids: Occurrence, Synthesis,
384 and Functions. *Annu. Rev. Biochem.* **61**, 517–57.
- 385 10 Bates, H. A., Kaushal, A., Deng, P. N. and Sciaky, D. (1984) Structure and synthesis of histopine, a
386 histidine derivative produced by crown gall tumors. *Biochemistry* **23**, 3287–3290.
- 387 11 Biemann, K., Lioret, C., Asselineau, J., Lederer, E. and Polonsky, J. (1960) On the structure of
388 lysopine, a new amino acid isolated from crown gall tissue. *Biochim. Biophys. Acta* **40**, 369–370.
- 389 12 Smits, S. H. J., Mueller, A., Schmitt, L. and Grieshaber, M. K. (2008) A Structural Basis for
390 Substrate Selectivity and Stereoselectivity in Octopine Dehydrogenase from *Pecten maximus*. *J.*
391 *Mol. Biol.* **381**, 200–211.
- 392 13 Van Thoai, N., Huc, C., Pho, D. B. and Olomucki, A. (1969) Octopine déshydrogénase : Purification
393 et Propriétés Catalytiques. *Biochim. Biophys. Acta BBA - Enzymol.* **191**, 46–57.
- 394 14 Chang, C.-C. and Chen, C.-M. (1983) Evidence for the presence of N^2 -(1,3-dicarboxypropyl)-L-
395 amino acids in crown-gall tumors induced by *Agrobacterium tumefaciens* strains 181 and EU6.
396 *FEBS Lett.* **162**, 432–435.
- 397 15 Chang, C.-C., Chen, C.-M., Adams, B. R. and Trost, B. M. (1983) Leucinopine, a characteristic
398 compound of some crown-gall tumors. *Proc. Natl. Acad. Sci. USA* **80**, 3573–3576.
- 399 16 Gäde, G., Weeda, E. and Gabbott, P. A. (1978) Changes in the Level of Octopine during the
400 Escape Responses of the Scallop, *Pecten maximus* (L.). *J. Comp. Physiol. B* **124**, 121–127.
- 401 17 Harcet, M., Perina, D. and Pleše, B. (2013) Opine Dehydrogenases in Marine Invertebrates.
402 *Biochem. Genet.* **51**, 666–676.
- 403 18 Moore, L. W., Chilton, W. S. and Canfield, M. L. (1997) Diversity of Opines and Opine-Catabolizing
404 Bacteria Isolated from Naturally Occurring Crown Gall Tumors. *Appl. Environ. Microbiol.* **63**, 201–
405 207.
- 406 19 Dessaux, Y. and Faure, D. (2018) Niche Construction and Exploitation by *Agrobacterium*: How to
407 Survive and Face Competition in Soil and Plant Habitats. In *Agrobacterium Biology: From Basic*
408 *Science to Biotechnology* (Gelvin, S. B., ed.), pp 55–86, Springer International Publishing, Cham.
- 409 20 Tremblay, G., Gagliardo, R., Chilton, W. S. and Dion, P. (1987) Diversity among Opine-Utilizing
410 Bacteria: Identification of Coryneform Isolates. *Appl. Environ. Microbiol.* **53**, 1519–1524.
- 411 21 Lang, J., Vigouroux, A., Planamente, S., Sahili, A. E., Blin, P., Aumont-Nicaise, M., Dessaux, Y.,
412 Moréra, S. and Faure, D. (2014) *Agrobacterium* Uses a Unique Ligand-Binding Mode for Trapping
413 Opines and Acquiring A Competitive Advantage in the Niche Construction on Plant Host. *PLOS*
414 *Pathog.* **10**, e1004444.
- 415 22 Montoya, A. L. (1977) Octopine and Nopaline Metabolism in *Agrobacterium tumefaciens* and
416 Crown Gall Tumor Cells: Role of Plasmid Genes. *J. Bacteriol.* **129**, 101–107.

- 417 23 Grim, K. P., San Francisco, B., Radin, J. N., Brazel, E. B., Kelliher, J. L., Párraga Solórzano, P. K.,
418 Kim, P. C., McDevitt, C. A. and Kehl-Fie, T. E. (2017) The Metallophore Staphylopin Enables
419 *Staphylococcus aureus* To Compete with the Host for Zinc and Overcome Nutritional Immunity.
420 mBio (Torres, V. J., ed.) **8**.
- 421 24 Remy, L., Carrière, M., Derré-Bobillot, A., Martini, C., Sanguinetti, M. and Borezée-Durant, E.
422 (2013) The *Staphylococcus aureus* Opp1 ABC transporter imports nickel and cobalt in zinc-
423 depleted conditions and contributes to virulence: Nickel and cobalt uptake in *Staphylococcus*
424 *aureus*. Mol. Microbiol. **87**, 730–743.
- 425 25 Fojcik, C., Arnoux, P., Ouerdane, L., Aigle, M., Alfonsi, L. and Borezée-Durant, E. (2018)
426 Independent and cooperative regulation of staphylopin biosynthesis and trafficking by Fur and
427 Zur: Regulation of *S. aureus cnt* operon by Fur and Zur. Mol. Microbiol. **108**, 159–177.
- 428 26 Mastropasqua, M. C., D’Orazio, M., Cerasi, M., Pacello, F., Gismondi, A., Canini, A., Canuti, L.,
429 Consalvo, A., Ciavardelli, D., Chirullo, B., et al. (2017) Growth of *Pseudomonas aeruginosa* in zinc
430 poor environments is promoted by a nicotianamine-related metallophore: Metallophore-
431 mediated zinc uptake in *Pseudomonas aeruginosa*. Mol. Microbiol. **106**, 543–561.
- 432 27 Bielecki, P., Puchałka, J., Wos-Oxley, M. L., Loessner, H., Glik, J., Kawecki, M., Nowak, M.,
433 Tümmler, B., Weiss, S. and dos Santos, V. A. P. M. (2011) In-Vivo Expression Profiling of
434 *Pseudomonas aeruginosa* Infections Reveals Niche-Specific and Strain-Independent
435 Transcriptional Programs. PLoS ONE (Brown, S. P., ed.) **6**, e24235.
- 436 28 Gi, M., Lee, K.-M., Kim, S. C., Yoon, J.-H., Yoon, S. S. and Choi, J. Y. (2015) A novel siderophore
437 system is essential for the growth of *Pseudomonas aeruginosa* in airway mucus. Sci. Rep. **5**,
438 14644.
- 439 29 Ding, Y., Fu, Y., Lee, J. C. and Hooper, D. C. (2012) *Staphylococcus aureus* NorD, a Putative Efflux
440 Pump Coregulated with the Opp1 Oligopeptide Permease, Contributes Selectively to Fitness *In*
441 *Vivo*. J. Bacteriol. **194**, 6586–6593.
- 442 30 Altschul, S. F., Madden, T. L., Schäffer, A. A., Zhang, J., Zhang, Z., Miller, W. and Lipman, D. J.
443 (1997) Gapped BLAST and PSI-BLAST: a new generation of protein database search programs.
444 Nucleic Acids Res. **25**, 3389–3402.
- 445 31 Edgar, R. C. (2004) MUSCLE: multiple sequence alignment with high accuracy and high
446 throughput. Nucleic Acids Res. **32**, 1792–1797.
- 447 32 Clamp, M., Cuff, J., Searle, S. M. and Barton, G. J. (2004) The Jalview Java alignment editor.
448 Bioinformatics **20**, 426–427.
- 449 33 Vallenet, D., Belda, E., Calteau, A., Cruveiller, S., Engelen, S., Lajus, A., Le Fèvre, F., Longin, C.,
450 Mornico, D., Roche, D., et al. (2013) MicroScope—an integrated microbial resource for the
451 curation and comparative analysis of genomic and metabolic data. Nucleic Acids Res. **41**, D636–
452 D647.
- 453 34 Hajjar, C., Fanelli, R., Laffont, C., Brutesco, C., Cullia, G., Tribout, M., Nurizzo, D., Borezée-Durant,
454 E., Voulhoux, R., Pignol, D., et al. (2019) Control by Metals of Staphylopin Dehydrogenase
455 Activity during Metallophore Biosynthesis. J. Am. Chem. Soc. **141**, 5555–5562.
- 456 35 Higuchi, K., Kanazawa, K., Nishizawa, N.-K. and Mori, S. (1996) The role of nicotianamine
457 synthase in response to Fe nutrition status in Gramineae. Plant Soil **178**, 171–177.
- 458 36 Wilks, H. M., Hart, K. W., Feeney, R., Dunn, C. R., Muirhead, H., Chia, W. N., Barstow, D. A.,
459 Atkinson, T., Clarke, A. R. and Holbrook, J. J. (1988) A specific, highly active malate
460 dehydrogenase by redesign of a lactate dehydrogenase framework. Science **242**, 1541–1544.
- 461 37 Müller, A., Janßen, F. and Grieshaber, M. K. (2007) Putative reaction mechanism of
462 heterologously expressed octopine dehydrogenase from the great scallop, *Pecten maximus* (L).
463 FEBS J. **274**, 6329–6339.
- 464 38 Vigouroux, A., El Sahili, A., Lang, J., Aumont-Nicaise, M., Dessaux, Y., Faure, D. and Moréra, S.
465 (2017) Structural basis for high specificity of octopine binding in the plant pathogen
466 *Agrobacterium tumefaciens*. Sci. Rep. **7**.
- 467 39 Alloway, B. J. (2009) Soil factors associated with zinc deficiency in crops and humans. Environ.
468 Geochem. Health **31**, 537–548.

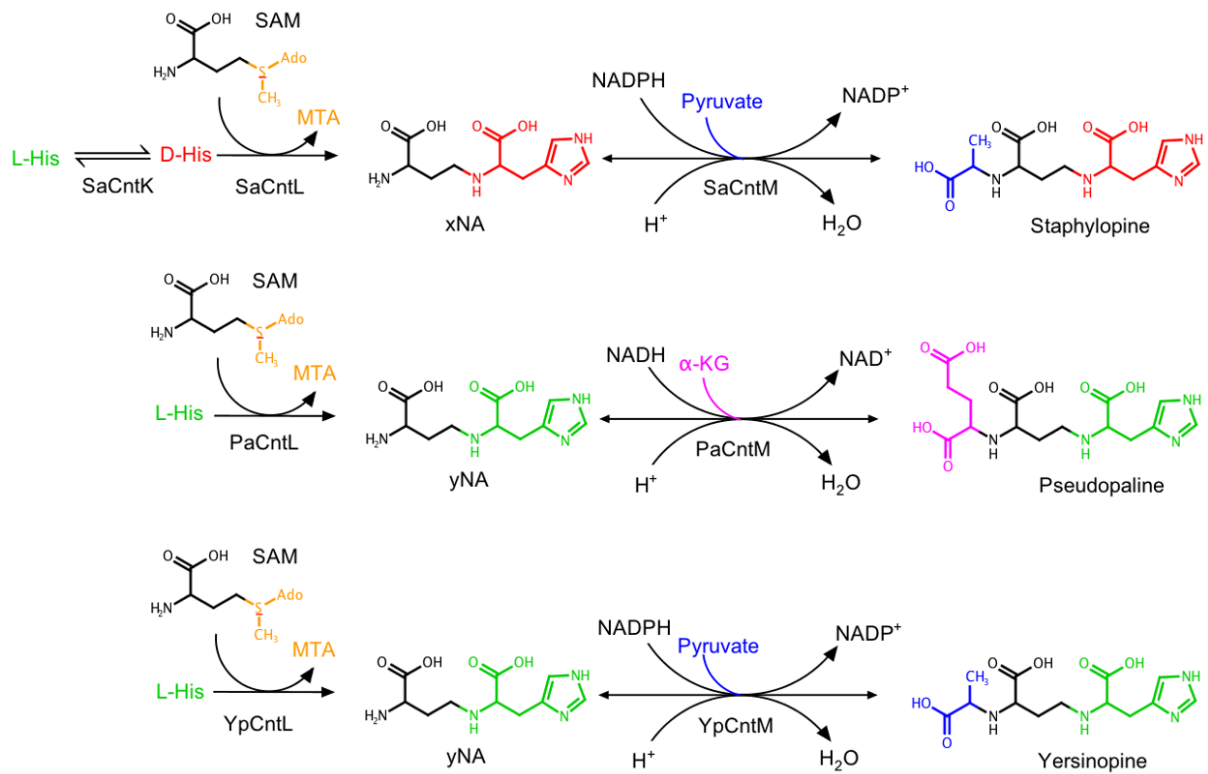
- 469 40 Deng, S., Bai, R., Hu, X. and Luo, Q. (2003) Characteristics of a bioflocculant produced by *Bacillus*
470 *mucilaginosus* and its use in starch wastewater treatment. *Appl. Microbiol. Biotechnol.* **60**, 588–
471 593.
- 472 41 Goswami, D., Parmar, S., Vaghela, H., Dhandhukia, P. and Thakker, J. N. (2015) Describing
473 *Paenibacillus mucilaginosus* strain N3 as an efficient plant growth promoting rhizobacteria
474 (PGPR). *Cogent Food Agric.* (Moral, M. T., ed.) **1**.
- 475 42 Liu, S., Tang, W., Yang, F., Meng, J., Chen, W. and Li, X. (2017) Influence of biochar application on
476 potassium-solubilizing *Bacillus mucilaginosus* as potential biofertilizer. *Prep. Biochem.*
477 *Biotechnol.* **47**, 32–37.
- 478 43 Haas, D. and Défago, G. (2005) Biological control of soil-borne pathogens by fluorescent
479 *pseudomonads*. *Nat. Rev. Microbiol.* **3**, 307–319.
- 480

481

482 **Figures and figure legends**

483

484

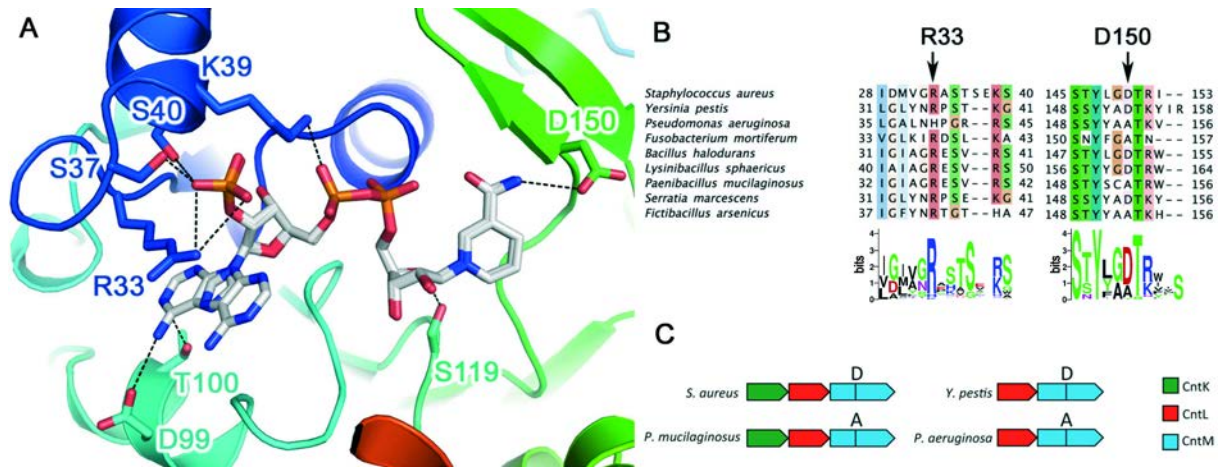


485

486 Figure 1: Differences in the staphylopin, pseudopaline, and yersinopine biosynthetic pathways.

487 Adapted from [5,6,8].

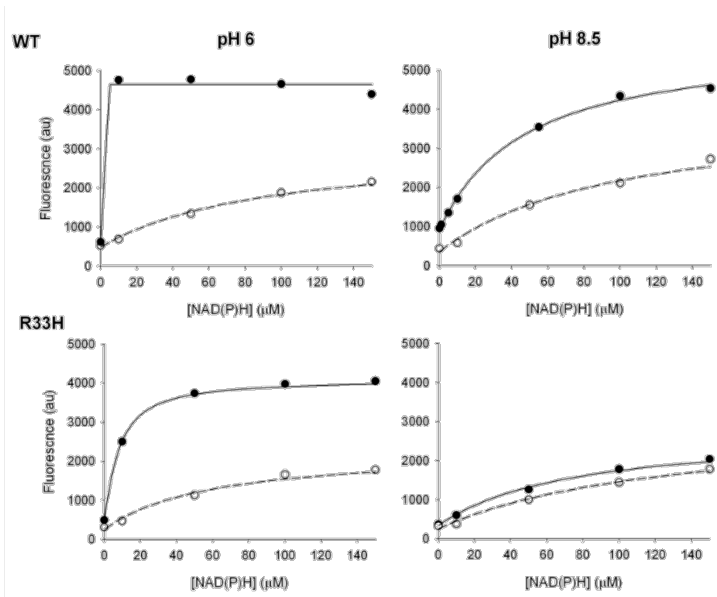
488



489
 490 Figure 2: CntM structure, sequence conservation around NADPH and operon diversity highlight
 491 protein selectivity. (A) Details of the NADPH binding site on SaCntM with side chains of residues
 492 located up to 4Å around the NADPH represented in stick. The protein is colored from N-terminus
 493 (blue) to C-terminus (red). The pdb code used for this figure corresponds to 6H3D and shows two
 494 alternative positions for the adenine moiety of NADPH. Dashed lines indicate hydrogen bonds and salt
 495 bridges. The nicotinamide moiety is where the reductive condensation of xNA with pyruvate occurs
 496 and is involved in a putative hydrogen bond with D150 side chain. (B) Sequence alignment of nine
 497 CntM protein sequences from bacteria. Threshold for the Clustal coloring scheme correspond to 30 %
 498 sequence conservation as defined in Jalview. Arrows point to residues involved in NADPH/NADH
 499 selectivity and pyruvate/ α -ketoglutarate selectivity. A weblogo representation of the entire unitprot
 500 family available from Pfam (318 entries) is drawn below the alignment, showing the conservation of
 501 position equivalent to R33 (R: 90%, H: 6% and K: 4%) and D150 (D: 72%, A: 25% and T: 3%) (C)
 502 Genomic organization of the biosynthetic genes of four different *cnt* operons in bacteria.

503

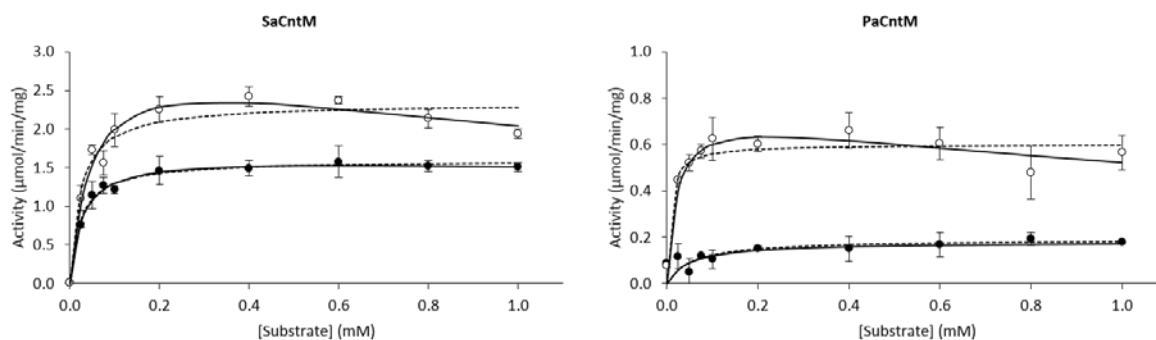
504



505
 506 Figure 3: Titration of NADPH (black circles) and NADH (white circles) binding to SaCntM (5 μ M) at
 507 pH = 6.0 or pH = 8.5 followed by fluorescence energy transfer between tryptophan excitation (280
 508 nm) and NAD(P)H emission (450 nm).

509

510



511
 512 Figure 4: Activity profile of SaCntM and PaCntM using variable concentrations of xNA (black circle)
 513 and yNA (white circle) with fixed concentrations of other substrates: 0.2 mM of NADPH and 1 mM of
 514 pyruvate when evaluating SaCntM, or 0.2 mM of NADH and 1 mM of α -ketoglutarate when
 515 evaluating PaCntM. The data points are means of three replicates with standard deviations. The fits are
 516 made using the Michaelis-Menten model considering (continuous line) or not (dashed line) a substrate
 517 inhibition.

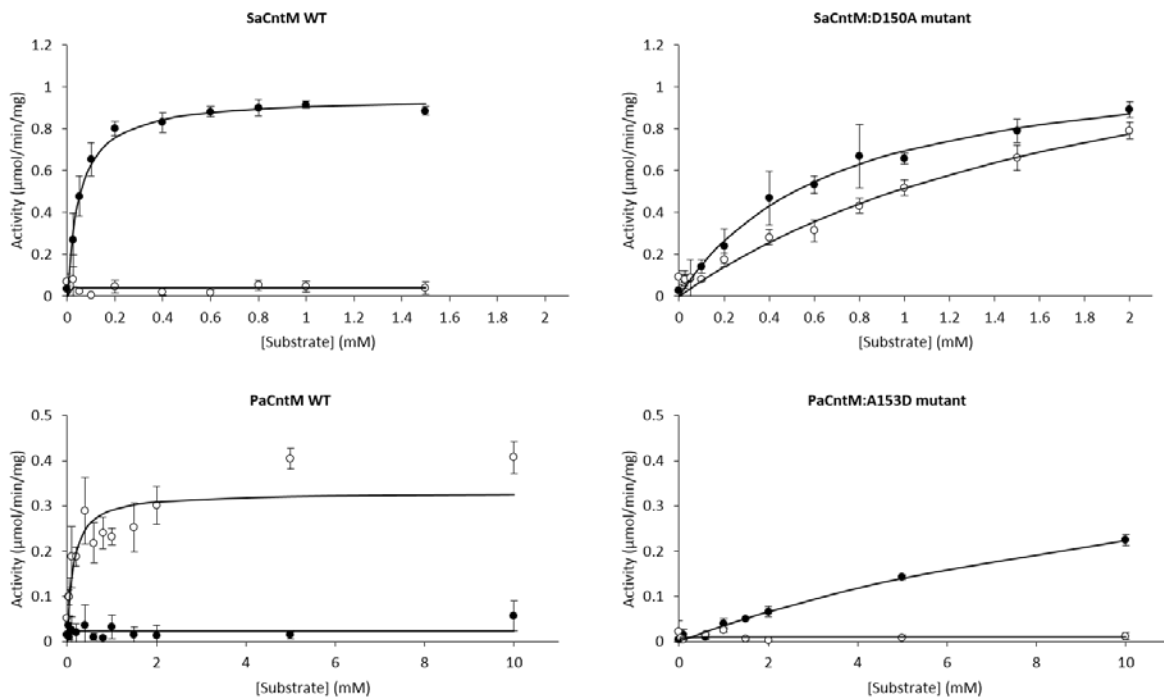
518

519

Protein	xNA vs yNA	K_m (μM)	K_i (mM)	k_{cat} (s^{-1})	k_{cat}/K_m ($\text{M}^{-1}\text{s}^{-1}$)
SaCntM	yNA	47 ± 9	2.3 ± 0.8	3.18 ± 0.25	67 584
SaCntM	xNA	23 ± 3	NA	1.67 ± 0.04	72 711
PaCntM	yNA	21 ± 7	2.4 ± 1.0	0.62 ± 0.06	29 618
PaCntM	xNA	54 ± 20	NA	0.16 ± 0.02	2 918

520 Table 1: Kinetic parameters of SaCntM and PaCntM activities established for a concentration range of
521 xNA and yNA with fixed concentrations of other substrates: 0.2 mM of NADPH and 1 mM of
522 pyruvate when evaluating SaCntM, and 0.2 mM of NADH and 1 mM of α -ketoglutarate when
523 evaluating PaCntM. The data and the standard errors associated with were generated by SigmaPlot
524 according to the Michaelis-Menten model with or without substrate inhibition. (NA: Not Applicable;
525 V_m : Maximum velocity; K_m : Michaelis constant; K_i : Inhibition constant; k_{cat} : Catalytic constant (or
526 turnover number); k_{cat}/K_m : Catalytic efficiency).

527



528
 529 Figure 5: Activity profile of SaCntM (WT and D150A mutant) and PaCntM (WT and A153D mutant)
 530 using variable concentrations of pyruvate (black circle) and α -ketoglutarate (white circle) with fixed
 531 concentrations of others substrates: 0.2 mM of NADPH and xNA when evaluating SaCntM, and 0.2
 532 mM of NADH and yNA when evaluating PaCntM. The data points are means of three replicates with
 533 standard deviations. The fits are made using the Michaelis-Menten model.

534

Protein	Pyruvate vs αKG	K_m (μM)	k_{cat} (s^{-1})	k_{cat}/K_m ($M^{-1}s^{-1}$)
SaCntM	pyruvate	51 ± 6	1.00 ± 0.02	19 592
SaCntM	α KG	ND	0.04 ± 0.01	ND
SaCntM:D150A	pyruvate	$681 \pm 115^*$	$1.23 \pm 0.08^*$	1 807*
SaCntM:D150A	α KG	$2\,040 \pm 431^*$	$1.65 \pm 0.22^*$	809*
PaCntM	pyruvate	ND	0.02 ± 0.01	N.D.
PaCntM	α KG	133 ± 39	0.27 ± 0.02	2 058
PaCntM:A153D	pyruvate	$14\,986 \pm 2964^*$	$0.46 \pm 0.07^*$	31
PaCntM:A153D	α KG	ND	0.01 ± 0.01	ND

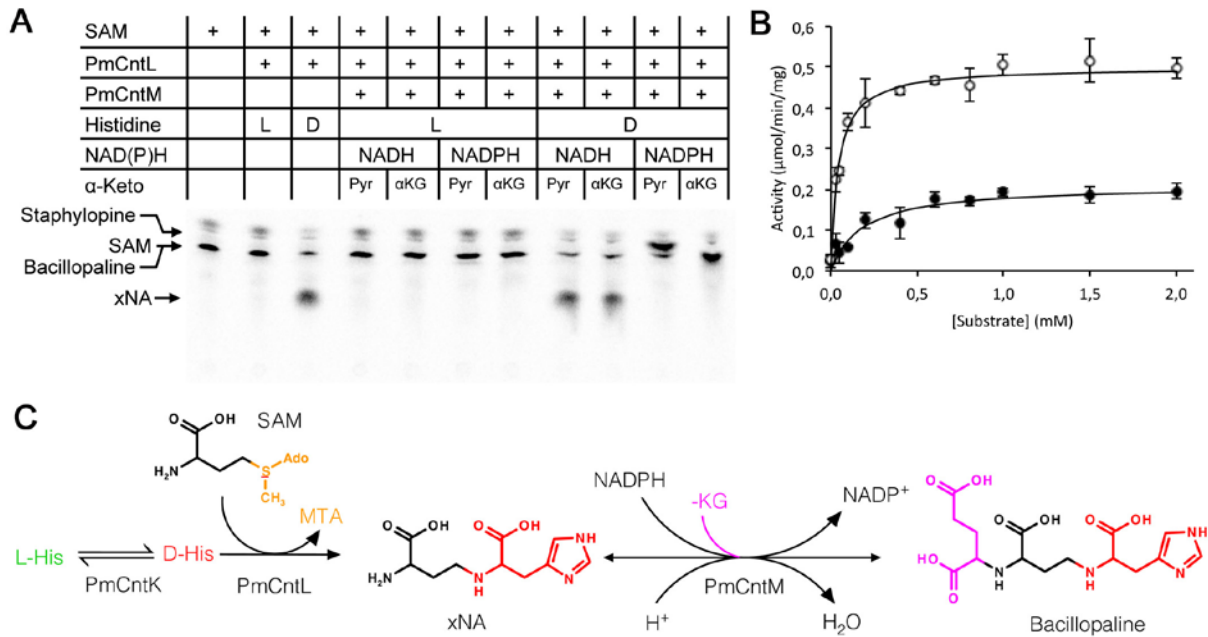
535 Table 2: Kinetic parameters of SaCntM (WT and D150A mutant) and PaCntM (WT or A153D
536 mutant) activities established for a concentration range of pyruvate and α KG with fixed concentrations
537 of other substrates: 0.2 mM of NADPH and xNA when evaluating SaCntM, and 0.2 mM of NADH
538 and yNA when evaluating PaCntM. The data and the standard errors associated with were generated
539 by SigmaPlot according to the Michaelis-Menten model. (ND: Not Determined). *Because the
540 maximum enzyme activity is not reached, these values are not well defined and must be taken with
541 caution.

542

543

544

545



546

547 Figure 6: Activity of CntL and CntM from *Paenibacillus mucilaginosus*. (A) TLC separation of
 548 reaction products incubating carboxyl- ^{14}C -labeled with purified enzyme (PmCntL and PmCntM) and
 549 various substrates (L-His (L) or D-His (D), pyruvate (Pyr) or α -ketoglutarate (α KG), NADH or
 550 NADPH). (B) Activity profile of PmCntM using variable concentrations of pyruvate (black circle) and
 551 α -ketoglutarate (white circle) with fixed concentrations of others substrates: 0.2 mM of NADPH and
 552 0.2 mM of xNA. The data points are means of three replicates with standard deviations. The fits are
 553 made using the Michaelis-Menten model. (C) Biosynthetic pathway for the assembly of bacillopaline
 554 from D-His, SAM and α -ketoglutarate.

555

Protein	Pyruvate vs αKG	K_m (μM)	k_{cat} (s^{-1})	k_{cat}/K_m ($M^{-1}s^{-1}$)
PmCntM	pyruvate	180 ± 39	0.18 ± 0.01	1 016
PmCntM	α KG	42 ± 5	0.44 ± 0.01	10 367

556 Table 3: Kinetic parameters of PmCntM activities established for a concentration range of pyruvate
557 and α KG with fixed concentrations of others substrates: 0.2 mM of NADPH and 0.2 mM of xNA. The
558 data and the standard errors associated with were generated by SigmaPlot according to the Michaelis-
559 Menten model.